DOI: 10.1002/chem.200501403

Effective Manipulation of the Electronic Effects and Its Influence on the Emission of 5-Substituted Tris(8-quinolinolate) Aluminum(III) Complexes

Victor A. Montes,[a] Radek Pohl,[a] Joseph Shinar,[b] and Pavel Anzenbacher, Jr.*[a]

Abstract: The unique electron-transport and emissive properties of tris-(8-quinolinolate) aluminum(III) (Alq_3) have resulted in extensive use of this material for small molecular organic light-emitting diode (OLED) fabrication. So far, efforts to prepare stable and easy-to-process red/green/blue (RGB)-emitting Alq_3 derivatives have met with only a limited success. In this paper, we describe how the electronic nature of various substituents, projected via an arylethynyl or aryl spacer to the position of the highest HOMO density (C5), may be used for effective emission tuning to obtain blue-, green-, and red-emitting materials. The synthetic strategy consists of four different pathways for the attachment of electron-donating and electron-withdrawing aryl or arylethynyl substituents to the 5-position of the quinolinolate ring. Successful tuning of the emission color covering the whole visible spectrum ($\lambda = 450$–800 nm) was achieved. In addition, the photophysical properties of the luminophores were found to correlate with the Hammett constant of the respective substituents, providing a powerful strategy with which to predict the optical properties of new materials. We also demonstrate that the electronic nature of the substituent affects the emission properties of the resulting complex through effective modification of the HOMO levels of the quinolinolate ligand.

Keywords: aluminum · electronic structure · organic light-emitting diodes · quinolinolate · semiconductors

Organic light-emitting diodes (OLEDs) are a promising technology for fabrication of full-color flat-panel displays,[1,2] and some are already being commercialized.[3] Nevertheless, a widespread use of OLED-based displays relies on wide availability of stable materials emitting red/green/blue (RGB) light of high color purity. Electroluminescent organometallic complexes are valued emitters for the fabrication of the so-called small-molecule OLEDs (SMOLEDs). Their advantages are, in general, good emission-color purity, their availability both as singlet[4] or triplet emitters,[5] and their ease of deposition by means of thermal vacuum evaporation. A major obstacle in the fabrication of SMOLED-based full-color displays so far appears to be the limited availability of long-lived complexes that cover the whole visible spectrum, while also possessing similar optoelectronic, semiconductor, and charge-transport properties.[1,2]

Success in the preparation of long-lasting SMOLED devices requires the careful design of materials possessing proper alignment of the HOMO/LUMO levels with other device components such as charge-injection and charge-transport layers in order to balance the mobility of the carriers and achieve efficient charge recombination in the emitting layer.[6] In undoped structures, the materials must also possess sufficiently large HOMO–LUMO gaps for the emission at the required wavelengths, high solid-state emission quantum yields, and high emission-color stability.

Since an early report in 1987,[7] tris(8-quinolinolate) aluminum(III) (Alq_3) has been used as an emitter and one of the most stable electron-transporting materials and host for saturated green and red colors currently used in SMOLEDs.[2,8] Although the past decade has seen great progress

[a] V. A. Montes, Dr. R. Pohl, Prof. P. Anzenbacher, Jr.
Department of Chemistry and Center for Photochemical Sciences
Bowling Green State University (BGSU)
Bowling Green, OH 43403 (USA)
Fax: (+1) 419-372-9809
E-mail: pavel@bgnet.bgsu

[b] Prof. J. Shinar
Ames Laboratory-USDOE and
Department of Physics and Astronomy
Iowa State University
Ames, IA 50011 (USA)

Supporting information for this article is available on the WWW under http://www.chemeurj.org/ or from the author. It contains details of the full synthesis and characterization of the precursors, ligands, and complexes; numeric values used to construct the energy-gap law correlations; and crystallographic data for **10c**,**d**,**j**, and **11h**.

in the preparation of hosts and emitters comparable to Alq_3, further improvement in both the efficiency and durability of OLED materials is still highly desirable.[9] Hence, we decided to investigate Alq_3-related materials in order to gain better understanding of the processes that may allow rational manipulation of the HOMO/LUMO levels in this fundamentally interesting and industrially important material.

Both the semiconductor and emissive properties are largely defined by the HOMO/LUMO levels of the quinolinolate ligand and its lowest electronic π–π* transitions.[10,11] A number of studies aimed at tuning the HOMO/LUMO levels and emission color in the Alq_3-type materials were attempted with a variable degree of success.[9] Physical and theoretical studies providing an insight into the distribution of the HOMO/LUMO densities in the quinolinolate ligand were also performed. According to density functional theory (DFT) calculations performed on *mer*-Alq_3,[10b–c] the HOMO orbitals are located mostly on the phenoxide side, and, in particular, at C5 of the ligand, whereas the highest LUMO density is found at the pyridine ring. It appears logical that substitution with suitable functional groups at the phenoxide ring would result in changes in the HOMO levels, and that the LUMO levels would be tuned by substituents on the pyridine ring.[12–13] However, the natural question as to whether substitution in a HOMO node or LUMO node would induce changes in both the HOMO *and* LUMO levels remained unanswered.

Previous attempts to modify Alq_3 by focusing mainly on manipulating the HOMO–LUMO gap (i.e., the emission energy) were motivated by the assumption that the substitution of electron-donating groups (EDGs) such as methyl at the 2-, 3-, and 4-positions of the quinolinolate ligand would induce a destabilizing effect on the LUMO, thus increasing the LUMO energy and the HOMO–LUMO gap. By the same token, substitution with electron-withdrawing groups (EWGs) at the 5-, 6-, and 7-positions should deplete the HOMO density, resulting in an increase in the energy of the π–π* transition and an emission that is blueshifted relative to the parent Alq_3 ($\lambda_{max} = 525$ nm).[9,12] Although this common-sense approach ought to provide a handle for tuning the complex emission, the literature does not provide evidence supporting this relationship between the electronic nature of the substituent and the emissive properties of the respective aluminum quinolinolate. In particular, the C5-substituted complexes, the most widely represented group of Alq_3 derivatives, do not show this correlation. The only notable example of blueshifted fluorescence in an Alq_3 derivative was obtained with the piperidyl amide of Alq_3-5-sulfonic acid with the emission maximum at $\lambda = 480$ nm.[14] Other attempts at emission tuning failed to yield significant effects or blue-emitting complexes. For example, the introduction of a cyano group at the 5-position of the quinolinolate resulted only in a 4 nm blueshift,[15] whereas the fluoro and chloro[16] substituents yielded, against expectations, Alq_3 complexes with slightly redshifted emissions of $\lambda = 535$ and 540 nm, respectively.

Perhaps the best example of a systematic effect on the complex emission is represented by the introduction of a (weakly electron-donating) methyl group into the quinolinolate ligand. When a methyl group is attached to the electron-deficient pyridyl ring it causes a blueshift in the emission (λ_{max} increases from 490 to 523 nm for positions 2 to 4, respectively), whereas substitution on the electron-rich phenoxide ring produces a redshift (λ_{max} increases from 525 to 568 nm for positions 5 to 7, respectively).[12,16–17] However, it should be noted that because of steric hindrance, the tris-aluminum(III) complex with 8-hydroxy-2-methylquinoline (the bluest emitter) is not stable, so one of the three quinolinolate ligands must be replaced by a smaller phenolato-type ligand, thus creating the pentacoordinate complexes instead.[1,18] Hence, one cannot be certain whether the dramatic blueshifted emission ($\lambda \approx 490$ nm) of the 8-hydroxy-2-methylquinoline complexes is due to methyl-mediated electronic tuning or simply to the less sterically favorable geometry of the 2-methylquinolinolate–aluminum(III) bonding.

Thus, the convoluted effects observed in the materials with the substituents attached directly to the quinolinolate ligand may be due to the competing resonance and inductive effects. In an effort to limit the direct mesomeric participation of substituent π electrons, in order to better understand the substituent effect on the energy and distribution of the HOMO and LUMOs and its possible use in the emission-color tuning in Alq_3 complexes, we decided to synthesize complexes **1a**–**k** and **2a**–**n**. The series comprise 5-substituted 8-quinoline ligands and various substituents connected by an arylethynyl or aryl spacer (see Figure 1).

In this paper, we describe how the electronic nature of various substituent groups, when projected through the selected spacers, allows for systematic tuning of the HOMO/LUMO levels and of the corresponding emission from the aluminum(III) quinolinolates.

Results and Discussion

Syntheses: The ligands and the corresponding Al^{III} complexes were prepared following previously published methods.[19,20] The hydroxyl group in the starting material, 5-bromo-8-hydroxyquinoline,[21] was protected by *t*-butyloxycarbonyl (Boc) or benzyl (Bn) protecting groups prior to the Pd-catalyzed coupling reactions. The Boc group shows excellent compatibility with the mild conditions for the Sonogashira–Hagihara cross-coupling used to attach the ethynyl-TMS (TMS = trimethylsilyl) and ethynylarenes to the quinolinolate (Scheme 1). Because the electron-rich (EDG) arenes do not undergo oxidative addition to Pd^0 as readily as electron-poor arenes, the EDG-substituted ethynylarenes were prepared separately and coupled to 5-Br-8-*O*-Boc-quinoline **3** in 60–82% yield. For the introduction of EWG arenes, quinoline **3** was first substituted with acetylene to give 8-*O*-Boc-5-ethynylquinoline **4** (obtained in two steps with 70% overall yield) followed by a cross-coupling reaction with suitable EWG bromoarenes to give **5a**,**b**,**d**–**f** (in

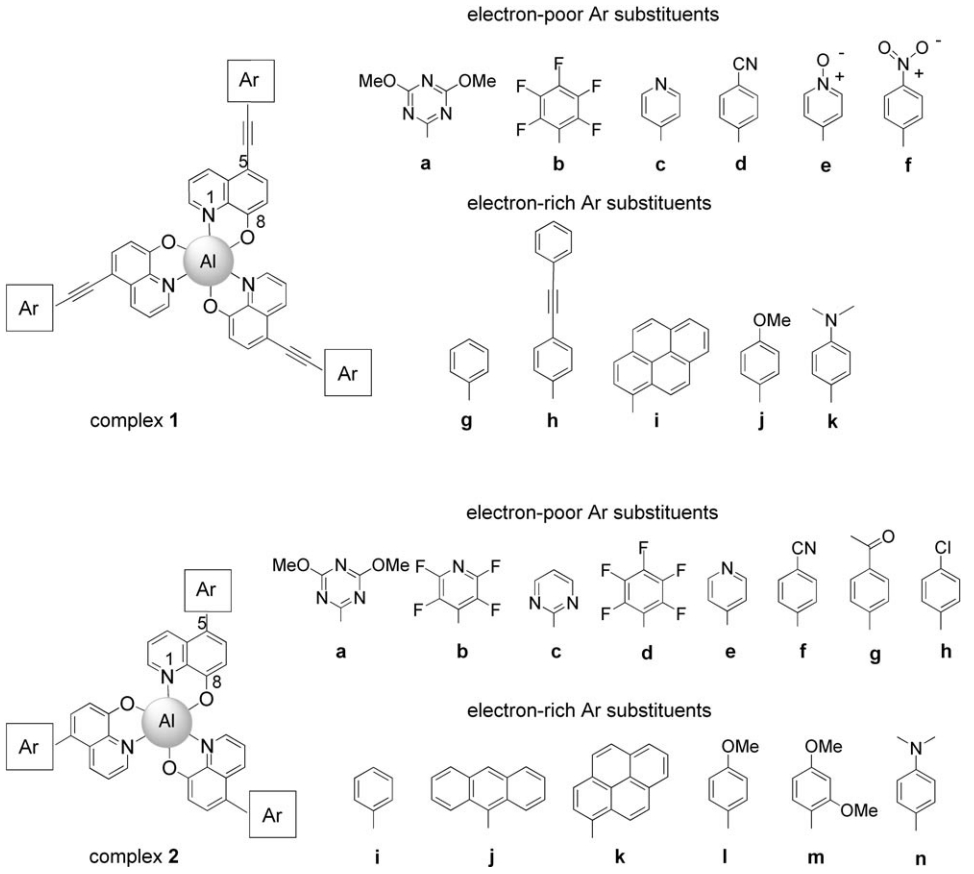

Figure 1. Structure of Alq_3 complexes **1a–k** and **2a–n** with electron-rich and electron-poor aromatic moieties.

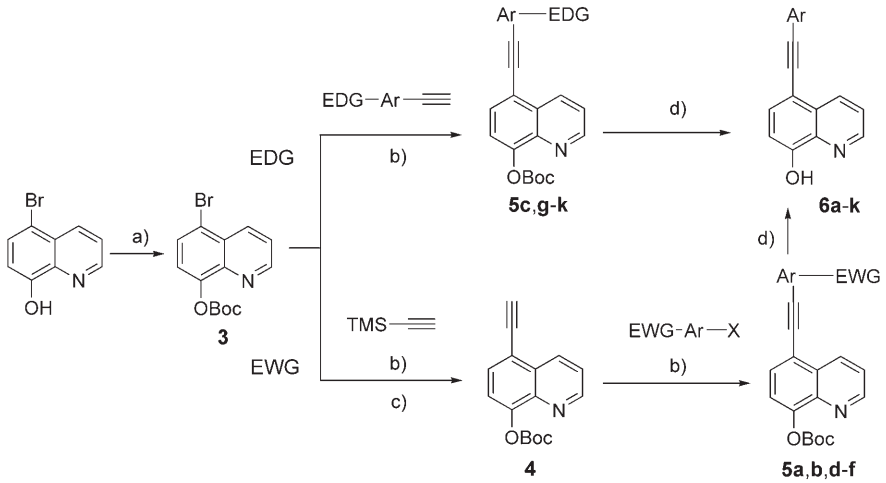

Scheme 1. Reaction conditions: a) di-*tert*-butyl dicarbonate, DMAP, hexane, RT, 5 h; b) $[Pd(PPh_3)_4]$ (5%), CuI (5%), DIPEA, THF, 60 °C, 24 h; c) KF (2 equiv), MeOH, RT, 3 h; d) piperidine (3 equiv), CH_2Cl_2, 5 min.

62–97% yield). The piperidine-promoted removal of the Boc group proceeds quantitatively, furnishing the free ligands **6a–k**.

The removal of the Boc group may also be accomplished by treatment of the Boc-protected intermediate with trifluoroacetate (TFA) resulting in crystalline TFA salts of the deprotected ligands. Unfortunately, with electron-rich aryl moieties attached to the ethynylene, lower yields of the deprotected TFA salts were obtained. This is due to the addition of TFA to the triple bond followed by hydrolysis as shown in Scheme 2. In the case of the dimethylamino-derivative **6k**, the resulting addition–hydrolysis product (25–30%) was isolated and its structure determined by using NMR and mass spectroscopies. The critical structural features in the NMR spectra of **7k** are characteristic signals for C=O (^{13}C NMR: $\delta = 194.5$ ppm) and $-CH_2-$ (^1H NMR: $\delta = 4.73$ ppm).

The presence of a strong base in the Suzuki–Miyaura coupling reaction (such as aqueous K_2CO_3) precluded using the hydrolytically unstable Boc group as protection, and the stable benzyl group was used to protect the 8-hydroxy group instead. The synthesis described in Scheme 3 employs an approach similar to the one described in Scheme 1. Here too, two different pathways were devised to attach the electron-rich EDG arenes by using previously prepared arene boronic acids in cross-coupling reactions with 8-benzyloxy-5-bromoquinoline **8**, while the introduction of electron-poor EWG arenes proceeded with higher yields when boronate ester **9** was cross-coupled to an EWG-substituted haloarene. The pinacolato boronate ester **9** was prepared by Pd^0-catalyzed borylation of **8** in 95% yield. Alternatively, the aryl–aryl cross-coupling may be achieved through a Stille reaction, in which intermediate **8** is reacted with a trialkylstannyl arene. This method, however, requires stannylarene intermediates, which are less readily available compared with a large number of commercially available boronic acids. Deprotection of the benzyl group was achieved by transfer hydrogenation using 1,4-cyclohexadiene as a hydrogen source.[22]

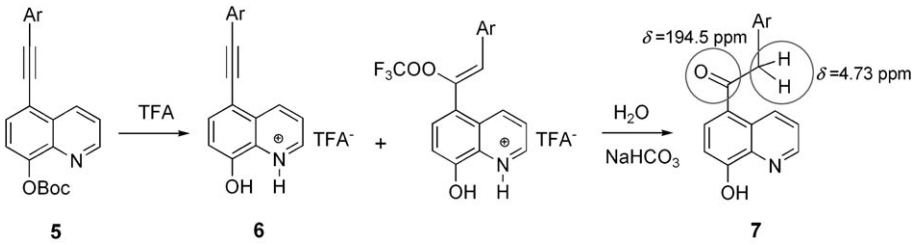

Scheme 2. Deprotection of electron-rich ligands **5** by TFA resulted in formation of carbonyl-containing impurities of general structure **7**. Values for characteristic signals from the NMR spectra of **7k** are shown (see text for more details).

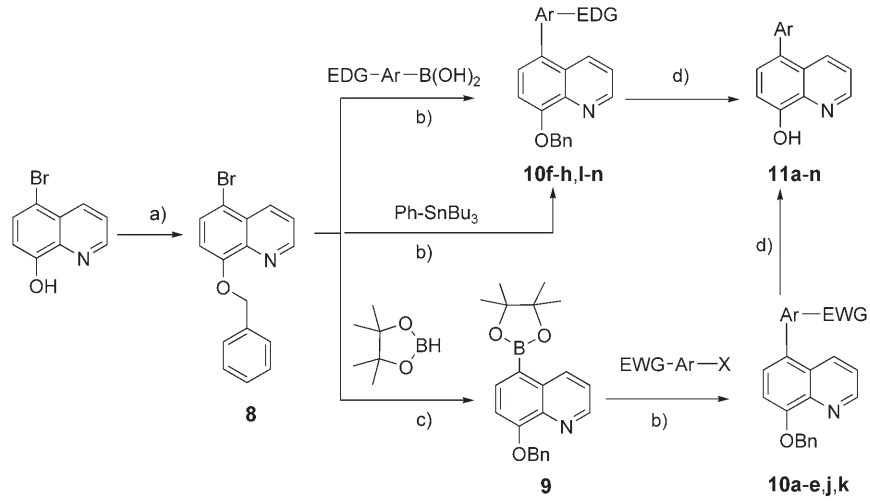

Scheme 3. Reaction conditions: a) Bn-Cl, K_2CO_3, CH_3CN, reflux, 16 h; b) $[Pd(PPh_3)_4]$ (5%), 1 M aq K_2CO_3, toluene, TBACl, 90 °C, 24 h; c) $[Pd(PPh_3)_4]$ (3%), Et_3N/THF, 100 °C, 24 h; d) 1,4-cyclohexadiene, Pd-C (10%), *i*PrOH, reflux, 3 h.

The final Al^{III} complexes **1a–k** and **2a–n** were obtained by reacting the deprotected ligands (free base or TFA salt) with $AlCl_3 \cdot 6H_2O$ in ethanol, followed by neutralization with triethylamine. The resulting complexes can exist as a mixture of two geometrical isomers, *fac* and *mer*, in the solid state.[23] Nevertheless, the *mer*-Alq_3 isomer is predicted to be more stable[10,24] and is the only species observed in solution due to rapid interconversion from the *fac* form.[25] Indeed, the ^1H NMR and ^{19}F NMR spectra recorded for complexes **1a–k** and **2a–n** support the presence of only one type of isomer in solution, with a magnetic environment consistent with the *mer* geometry (C_{3v} symmetry).[26]

Spectroscopic properties: The complexes **1a–k** and **2a–n** were studied by using UV-visible and fluorescence spectroscopies and the resulting data are summarized in Table 1. For both series, the π–π* absorption maxima of the complexes shifted to lower energies relative to the transition of the parent Alq_3 ($\lambda_{max}^{abs} = 388$ nm), presumably the result of an extension in the conjugation of the quinoline chromophore. As one could expect, the attachment of an aryl group onto a triple bond results in a higher degree of conjugation (lower π–π* transition energies) for the complexes **1a–k** relative to the aryl series **2a–n**. A higher oscillator strength relative to Alq_3 ($\varepsilon = 7 \times 10^3\ M^{-1}\,cm^{-1}$) was also observed for the extended chromophores in both series (**1** and **2**).

A simple visual examination of the photoluminescence upon excitation of sample solutions in dichloromethane with black light (365 nm) reveals successful color tuning, mediated by the arylethynyl and aryl electronic spacers (Figure 2). Despite the functional-group-mediated systematic tuning in the acetylene series, it appears that the through-the-bridge conjugation is perhaps too effective, resulting in relatively electron-rich species. We presume this to be the reason that precluded obtaining a significant blueshifted emission in the acetylene series. Nevertheless, the clearly observable substituent-mediated emission tuning observed for the first time in 5-substituted Alq_3 derivatives was encouraging.

We believed that the compounds of the aryl series (**2a–n**) with the electronic effectors attached directly to the quinolinolate fluorophore (i.e., without the acetylene bridge) would show amplified emission tuning. This hypothesis was confirmed by fluorescence spectra recorded for both the ethynylarene **1a–k** and aryl series **2a–n** compounds (Figure 2). In both series, the emission profiles cover a significant portion of the visible spectrum. The emission maxima for **1a–k** span $\lambda = 80$ nm (520–600 nm), whereas for the series **2a–n** they span $\lambda = 120$ nm (490–612 nm).

The photophysical data obtained from spectroscopic measurements of Alq_3 complexes **1a–k** and **2a–n** are summarized in Table 1. In both series, we observed a remarkable correlation between the photophysical properties and the electronic nature of the attached substituents. One can see that both the absorption and the emission shift systematically from blue to green, yellow, and red depending on the electronic nature of the modulator group. This attests to a fine balance of electronic communication between the quinolinolate fluorophores and the appended moieties, while suppressing direct mesomeric participation of substituent π electrons of the aryl substituent.

X-ray crystallographic structure determination for the ligands suggests that there is a higher degree of coplanarity for the arylethynyl derivatives than for the aryl compounds (see Figure 3). By the same token, the *ortho* interactions be-

Table 1. Photophysical properties[a] recorded for Alq_3 and complexes **1a–k** and **2a–n** in oxygen-saturated dichloromethane at 22 °C.

Complex	λ_{max}^{abs} (ε)[b]	λ_F [nm]	Φ_F[c]	τ_F [ns]
Alq_3	388 (7.0×10^3)	526	0.171	15.38
	C5-ethynylarene series			
1a	407 (3.5×10^4)	520	0.317	11.85
1b	410 (2.7×10^4)	538	0.228	8.67
1c	414 (2.4×10^4)	541	0.235	8.95
1d	414 (8.4×10^4)	545	0.203	6.61
1e	423 (1.0×10^4)	559	0.037	2.14
1f	429 (4.7×10^4)	573	0.003	–
1g	421 (2.2×10^4)	561	0.088	3.56
1h	421 (4.1×10^4)	561	0.092	3.30
1i	421 (1.8×10^4)	569	0.047	1.86
1j	385 (6.8×10^4)[d]	573	0.036	1.28
1k	425 (3.9×10^4)	600	0.009	0.89
	C5-aryl series			
2a	390 (2.7×10^4)	490	0.533	29.50
2b	410 (2.7×10^4)	501	0.511	23.01
2c	397 (2.0×10^4)	513	0.536	15.61
2d	388 (1.1×10^4)	516	0.453	20.31
2e	397 (7.5×10^3)	530	0.301	16.57
2f	398 (1.4×10^4)	534	0.298	14.53
2g	394 (1.4×10^4)	537	0.234	12.76
2h	402 (1.0×10^4)	541	0.201	11.13
2i	402 (1.0×10^4)	545	0.100	9.72
2j	389 (1.7×10^4)[d]	538	0.105	10.10
2k	385 (2.2×10^4)[d]	551	0.098	6.53
2l	410 (4.7×10^4)	564	0.057	4.73
2m	404 (9.8×10^4)	564	0.049	4.33
2n	422 (1.0×10^4)	612	0.008	1.49

[a] λ_{max}^{abs} = absorption maximum, λ_F = fluorescence maximum, Φ_F = fluorescence quantum yield, τ_F = fluorescence lifetime. [b] Units are [nm] ($M^{-1}cm^{-1}$). [c] Determined by using quinine sulfate (in 0.05 M H_2SO_4) as a standard. [d] Absorption maxima are dominated by the pyrene/anthracene chromophores.

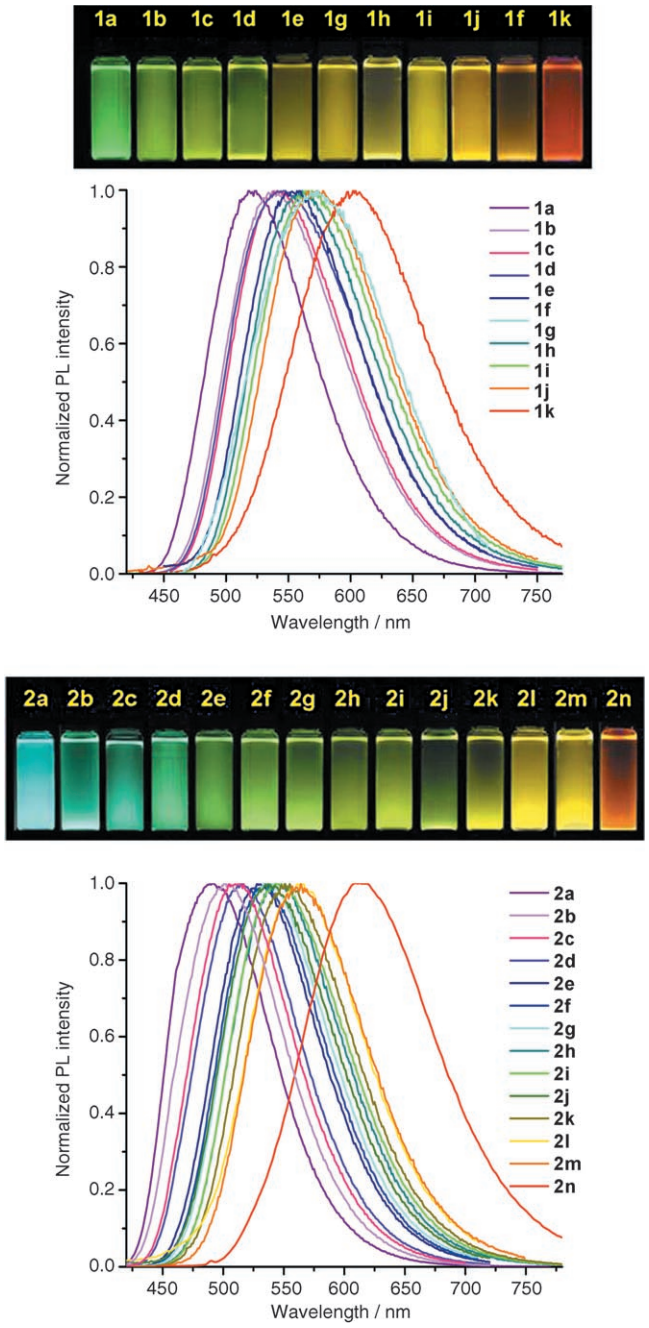

Figure 2. Emission of complexes **1a–k** and **2a–n** upon illumination with black light and the corresponding fluorescence spectra of complexes.

tween the aryl groups and quinoline reduce the degree of conjugation between the two moieties, which reduces the efficacy of electronic communication. Specifically, compound **5i**, in which the pyrene moiety is separated from quinoline by ethynylene, displays a 30° dihedral angle between the planes of quinoline and pyrene, whereas the angles between quinoline and the 2-pyrimidyl (**10c**), chlorophenyl (**11h**), pentafluorophenyl (**10d**), and 9-anthryl (**10j**) groups are 28, 50, 65, and 78°, respectively.

Close inspection of the data in Table 1 also shows that the fluorescence quantum yield and lifetime correlate with the electronic nature of the ligands. For the complexes bearing electron-poor substituents, the quantum yield and fluorescence lifetime were increased, whereas the electron-rich moieties resulted in a decrease in both the emission quantum yield and lifetime of the resulting complex with respect to a neutral substituent such as a phenyl group. In accordance with the energy-gap law,[27,28] analysis of the data confirmed an exponential dependence of the nonradiative-decay rate constant (k_{nr}) on the energy gap between the singlet and ground states, suggesting a uniform nature of the photophysical behavior in each series of complexes (see the Supporting Information for details). It is noteworthy that compounds **1e** and **1f** do not follow the trend in the arylethynyl series; this can be explained by considering that partial localization of the LUMO density on the nitro and pyridinium oxide moieties and alteration of the nature of the excited state take place.[13]

Furthermore, the fluorescence quantum yields and lifetimes exhibited excellent Hammett correlations with the constants σ_p.[29,30] This shows that the electronic effects are projected through the conjugated spacers to the quinolinolate emitter, thus providing an effective tool not only for systematic tuning of the photophysical properties, but also

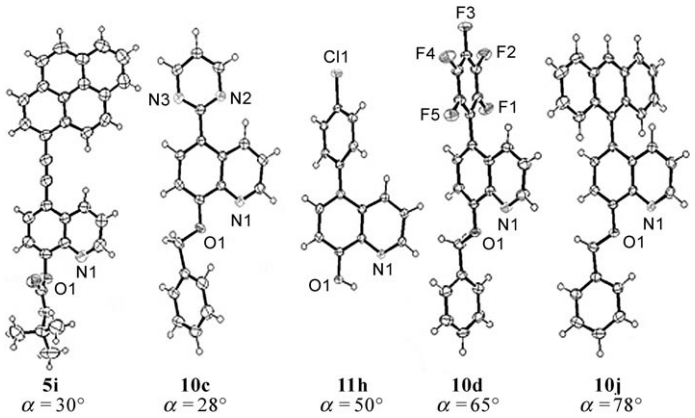

Figure 3. Single-crystal X-ray structures of compounds **5i**, **10c**, **11h, 10d**, and **10j** showing the difference in dihedral angle (α) between **5i** with an acetylene bridge and the compounds with an aryl–aryl bridge.

for predicting the properties of the complexes based on the Hammett correlation approach (Figure 4).

Electrochemical studies—estimation of HOMO/LUMO levels: Solution electrochemistry methods are known to provide insight into electron-transfer reactions in the condensed phase.[31a] The cyclic voltammogram of Alq_3 in solution is characterized by irreversible single reduction and oxidation processes. Experimental estimation of the HOMO–LUMO energy gap is in good agreement[32,33] with theoretical models.[10d] In order to achieve better understanding of the effect of the appended EWG/EDG moieties, we performed cyclic voltammetry (CV) measurements for complexes **1a–k** and **2a–n**. The main motivation, however, was not only to assess the energy gap of the materials, but to estimate the actual position of the HOMO and LUMO levels.

In both series **1a–k** and **2a–n**, we observed an electrochemical behavior similar to Alq_3.[32] Interestingly, the reduction process for the majority of the materials was observed to remain constant circa −1.9 V, whereas the oxidation process took place at voltages ranging from 0.27 to 1.32 V (Table 2). Also, in the derivatives with the most blue-shifted emission (**2a–d**), the oxidation process became difficult, an observation in accordance with the expected behavior of the more electron-deficient systems.

Table 2. Redox potentials, determined from cyclic voltammetry experiments,[a] of Alq_3 and derivatives **1a–k** and **2a–n**, and the calculated HOMO–LUMO gaps.

Complex	E^{ox} [V]	E^{red} [V]	HOMO–LUMO [eV]
Alq_3	1.02	−1.93	2.95
	C5-ethynylarene series		
1a	1.12	−1.96	3.08
1b	0.96	−1.93	2.89
1c	0.73	−1.94	2.67
1d	0.75	−1.89	2.64
1e	0.66	−1.90	2.56
1f	0.81	−1.64	2.45
1g	0.64	−1.89	2.53
1h	0.62	−1.93	2.55
1i	0.50, 1.10[b]	−1.85	2.35
1j	0.52, 1.18[b]	−1.83	2.35
1k	0.27, 0.52[b]	−1.93	2.20
	C5-aryl series		
2a	nd[c]	−1.93	nd[c]
2b	1.32	−1.86	3.18
2c	1.29	−1.82	3.11
2d	1.21	−1.91	3.12
2e	1.16	−1.91	3.07
2f	1.14	−1.93	3.07
2g	1.09	−1.88	2.97
2h	1.09	−1.94	3.03
2i	1.08	−1.90	2.98
2j	0.95[d]	−1.74[d]	nd[d]
2k	1.03[b] (br)	−1.92	2.95
2l	0.53, 1.04[b]	−1.94	2.47
2m	0.53, 0.97[b]	−1.94	2.47
2n	0.36, 0.53[b]	−1.94	2.30

[a] Measurements were performed in deoxygenated solutions of freshly distilled CH_2Cl_2 at room temperature. Potentials are reported against the ferrocene/ferrocenium redox couple (estimated error 50 mV). [b] According to literature reports, these additional peaks can be assigned to oxidation processes from pyrene, anisol, and dimethylaniline moieties.[31] [c] No detectable oxidation peak was observed. [d] Redox behavior attributed to the anthracene moiety. nd = not detected.[31a]

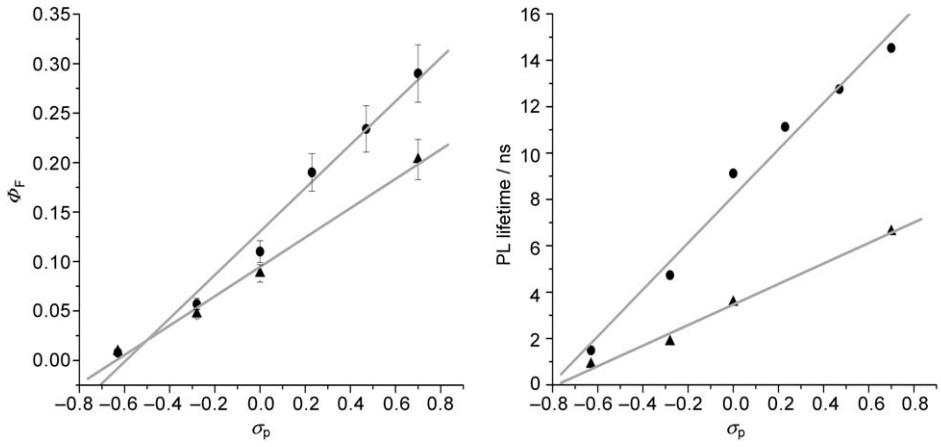

Figure 4. Hammett correlation of the quantum yield (left) and lifetime (right) for complexes **1d**,**g**,**j**,**k** (▲) and **2f–i**,**l**,**n** (●).

Because the actual HOMO and LUMO energy levels can be calculated from redox potentials by calibrating the scale of a reference to the zero vacuum level (Fermi level or absolute scale),[31a,34] we could estimate the frontier orbital energies for **1a–k** and **2a–n** (see the Supporting Information for details). In both series the LUMO was found to be largely unaffected throughout the series, and only the energy level of the HOMO was being

effectively manipulated. The data are shown in the graph in Figure 5.

These results represent unambiguous proof that the electronic properties of the moieties attached to the quinolino-

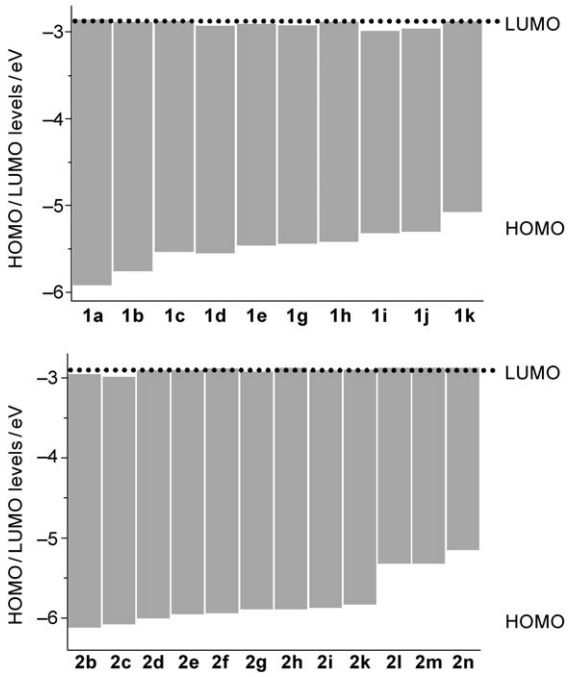

Figure 5. HOMO/LUMO energy levels calculated from the redox potentials of **1a–e**,**g–k** and **2b–i**,**k–n**.

late ligand through aryl and arylethynyl modulators are directly correlated with the position of the HOMO level of the complexes, supporting our initial notion for tuning the emission of Alq_3 derivatives through position C5, which has the highest HOMO density. Although it was expected that this approach may also lead to changes in the LUMO levels, surprisingly, the LUMO levels were unperturbed within the experimental error. Preserving the LUMO level in a more or less constant position is very important for homogeneous device manufacturing because these derivatives behave as electron-transport layers.

The HOMO–LUMO gaps calculated for **1a–k** and **2a–n** from electrochemical experiments show excellent correlation with the emission energies obtained from the photoluminescence (PL) spectra (see Figure 6). These data provide unequivocal confirmation not only of our structural design, but also of the photophysical nature of the tuning process.

OLED fabrication: The OLED fabrication was performed by using vacuum deposition and the typical architecture used for Alq_3.[35] The OLEDs were fabricated by using indium tin oxide (ITO)-coated glass substrates (150–200 nm; anode), copper phthalocyanine (5 nm), *N*,*N*′-diphenyl-*N*,*N*′-bis(1-naphthylphenyl)-1,1′-biphenyl-4,4′-diamine (60 nm), an Alq_3-type emitter (50 nm), a CsF (1 nm) buffer layer, and an Al cathode (150 nm).

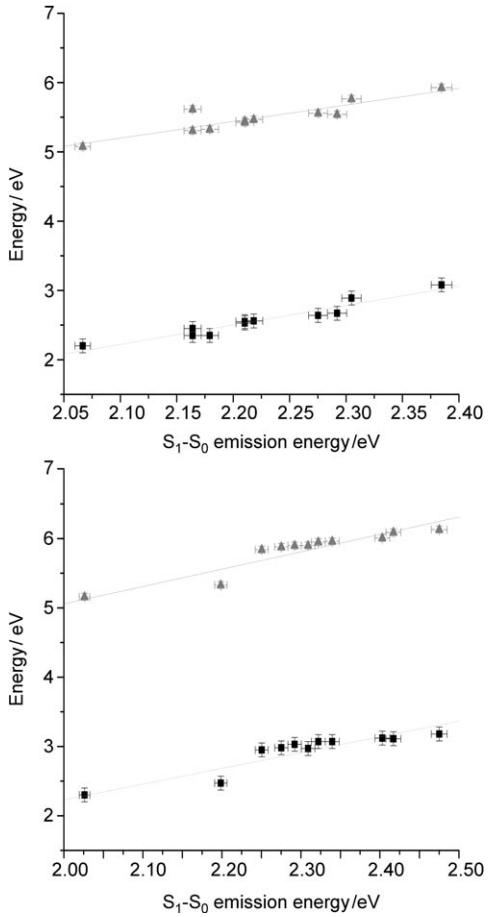

Figure 6. HOMO–LUMO gap (■) and HOMO level (▲) for **1a–k** and **2a–n** as a function of the fluorescence emission energy.

For derivatives that could not be thermally evaporated, the OLEDs were fabricated by means of spin coating: the ITO substrates were spun with poly(3,4-ethylenedioxythiophene)/poly(styrene sulfonate) (PEDOT/PSS) at 4000 rpm and were annealed at 150 °C for 60 min. The emitters were dissolved in a poly(9-vinylcarbazole) matrix (10 mg mL^{-1} in toluene) and spin coated at 2000 rpm onto the PEDOT/PSS. A 30 nm-thick layer of 2,9-dimethyl-4,7-diphenyl-1,10-phenanthroline (BCP) was then vacuum deposited onto the emitter layer, followed by the CsF and Al cathode.

Although we were originally concerned with the possible effect of the acetylene moiety on the stability of the actual devices, the OLEDs made of acetylene-substituted acenes[36] encouraged us to incorporate some of the acetylene-bearing materials in the OLEDs. Unfortunately, the thermal and electric stability of **1a–k** precluded their vacuum deposition, and the performance of the spin-coated devices was likewise unsatisfactory. We believe this to be due to the instability of the bridge triple bond. On the other hand, the performance of OLEDs fabricated by using complexes **2a–n** confirmed that these complexes are, indeed, electroluminophores, and, more importantly, that the electroluminescence (EL) spectra essentially reproduced the emission-tuning pattern observed in solution (Figure 7). Thus, the presence of electron-poor

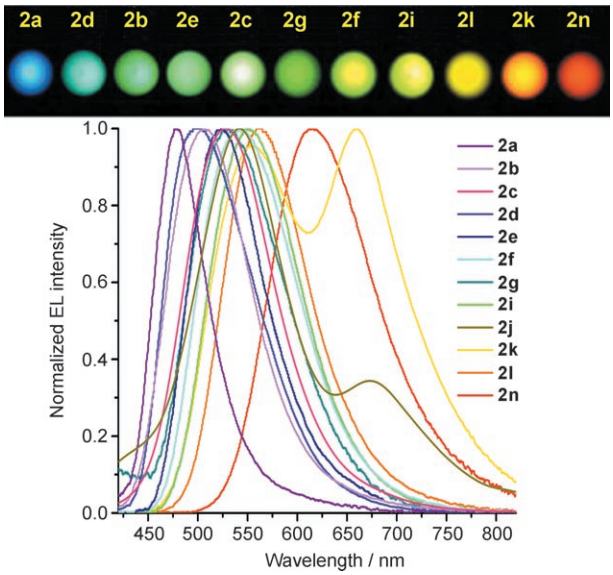

Figure 7. The OLEDs fabricated by using **2a**–**g**,**i**–**l**,**n** and the corresponding EL spectra confirm effective blue-to-red emission tuning in the solid state.

substituents resulted in blueshifted EL maxima whereas the presence of electron-rich groups resulted in redshifted EL.

Overall, the emission obtained from OLEDs fabricated from **2a**–**n** covered most of the visible region with the peak emission of the most blueshifted complex at $\lambda = 479$ nm (**2a**) and the most redshifted derivative centered at $\lambda = 616$ nm (**2n**). To the best of our knowledge, this represents the most blue- and redshifted emission obtained from Alq_3 host materials reported to date. Interestingly, the blueshifted emitting materials **2a**,**d**,**e** displayed slightly blueshifted EL maxima compared with the corresponding PL patterns (see Table 3). A similar but less pronounced effect was also observed for

Table 3. HOMO levels, photophysical data, and electroluminescence (EL) recorded for Alq_3 and complexes **2a**–**n**.

Complex	E^{HOMO} [eV]	λ_{PL} [nm]	λ_{EL}[a] [nm]	Φ_{PL}	Cd/A_{max}[b]	η_{max}[c]
Alq_3	5.85	526	520	0.171	2.57	0.83
2a	nd[d]	490	479	0.533	1.62	0.90
2b	6.13	501	505	0.511	0.31	0.12
2c	6.09	513	528	0.536	0.34	0.12
2d	6.01	516	500	0.453	0.69	0.29
2e	5.96	530	522	0.301	1.45	0.42
2f	5.95	534	541	0.298	1.24	0.38
2g	5.90	537	531	0.234	2.37	0.78
2h	5.90	541	531	0.201	0.04	0.01
2i	5.88	545	551	0.100	0.35	0.19
2j	5.75[e]	538	542/672	0.105	0.07	0.03
2k	5.84	551	555/660	0.098	1.01	0.30
2l	5.33	564	562	0.057	0.58	0.18
2m	5.33	564	nd[d]	0.049	nd[d]	nd[d]
2n	5.16	612	616	0.008	0.10	0.06

[a] The peak EL wavelength did not change significantly with applied voltage. [b] Maximum ratio between the forward-directed luminance of the device and the measured current density passing through the device. [c] Maximum external efficiency of the device. [d] Not detected. [e] Redox behavior attributed to anthracene moiety.[31a]

the green- and yellow-emitting devices based on **2g**,**h** and **2l**. OLEDs based on complexes **2j** and **2k** carrying 9-anthryl and 2-pyrenyl moieties showed a distinct emission profile with two components. In these cases, one of the EL maxima resembles the observed fluorescence spectra while the second lower-energy transition suggests exciplex emission generated between anthracene or pyrene moieties from the Alq_3 derivatives and the triarylamine (α-NPD) from the hole-transporting layer (see Figure 8). This hypothesis was

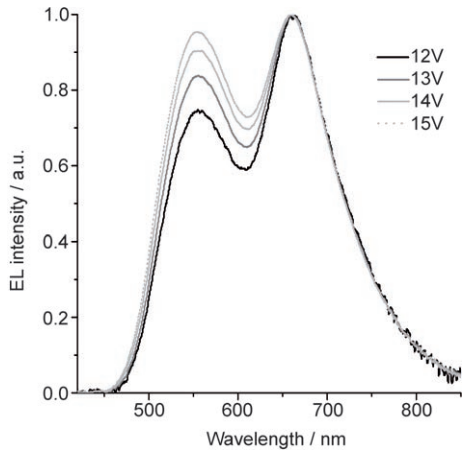

Figure 8. Electroluminescence dependence on voltage for the OLED based on **2k**.

indirectly supported by co-spin coating the respective complexes with α-NPD and recording solid-state PL spectra, which also showed similar bimodal patterns. In the absence of α-NPD, the films from **2j** and **2k** showed only one-component emission in agreement with their recorded solution spectra. In the OLEDs, the relative peak intensity of the exciplex maxima decreases with increased driving voltage. This is explained by moving the charge-recombination zone from the emitter–HTL (HTL = hole-transporting layer) interface with increasing voltage. Efforts toward utilizing this feature in the design of OLEDs emitting white light are currently being investigated.

The luminance and efficiency of the OLEDs based on **2a**–**n** were generally lower than that of homogeneous Alq_3 devices (see Table 3). The slightly inferior performance for devices constructed with our materials can be attributed to a number of reasons. In particular, the misalignment of the HOMO levels between the employed hole-transport layer (for α-NPD $E^{HOMO} = 5.40$ eV, for PEDOT/PSS $E^{HOMO} = 4.90$ eV)[14b,37] and the materials **2a**–**f** with EWG ($E^{HOMO} = 5.95$–6.13 eV for **2a**–**f**) would hinder hole injection into the emitter material, shifting the recombination zone towards the interface with the hole-transport layer thus lowering the EL efficiency. Likewise, in electron-rich complexes, low emission quantum yields would be a direct result of the energy-gap law dependence. Also, an exciplex formation leading to new redshifted emission bands also reduces the

efficiency of the devices. In spite of the fact that the OLED architecture and components were not performance optimized for the new materials, two derivatives, **2a** and **2f**, show a performance comparable to Alq_3 that is particularly significant for the blue **2a**-based OLED due to the scarcity of stable efficient blue emitters and hosts. Furthermore, the EL performance of these materials could be enhanced by introducing a different hole-transporting material with suitable ionization potentials so as to favor recombination of holes and electrons in the emitter layer. Individual optimization of the devices by using combinatorial matrix array techniques[38] is expected to yield devices with significantly higher performance.

Conclusion

The synthesis, optical properties, electrochemistry, electroluminescence, and OLED performance of a series of 5-substituted tris(8-quinolinolate) aluminum(III) complexes bearing ED/EW groups connected through aryl or arylethynyl moieties were described. Four pathways based on Sonogashira–Hagihara and Suzuki–Miyaura methodologies were devised to carry out the preparation of materials of diverse electronic nature in a simple yet effective fashion. From the spectroscopic measurements, it was shown that the substituent electronic effects, when projected to the quinolinolate chromophore via the selected conjugated spacers, provide an effective tool for a remarkable and systematic tuning of the emission over $\lambda = 350$ nm (450–800 nm). Additionally, the correlation between the electronic nature of the substituents and the emissive properties of the complexes suggests that our strategy may be used even to predict the properties of new Alq_3-based electroluminescent materials.

The HOMO–LUMO gaps estimated for **1a–k** and **2a–n** from electrochemical studies are in agreement with the emission energies obtained from the photoluminescence spectra. More importantly, the calculated levels for the frontier orbitals obtained demonstrated that the HOMO level was effectively manipulated, while the LUMO level was found to be largely unaffected in both series of derivatives. In conjunction, these results confirm the hypothesis that the electronic properties of the moieties attached to the quinolinolate ligand through aryl and arylethynyl modulators are directly correlated with the position of the HOMO level of the complexes.

Finally, OLED fabrication using materials **2a–n**, comprising an aryl group as an electronic spacer, was successfully achieved and the resulting devices displayed strong electroluminescence. Their spectra essentially reproduced the emission-tuning pattern observed in solution suggesting that this approach may be used to generate potentially useful electron-transporting and emissive OLED materials that could act either as energy hosts for guest dyes or as red/green/blue (RGB) emitters. This work has given insight into the design criteria for the development of potentially useful Alq_3-based materials and OLEDs.

Experimental Section

General: Commercially available solvents and reagents were used as received from the chemical suppliers. Reactions that required anhydrous conditions were carried out under an inert atmosphere of argon in oven-dried glassware. Tetrahydrofuran (THF) was distilled from a K-Na alloy under argon, and dichloromethane (CH_2Cl_2) was distilled from CaH_2 under argon. All reactions were monitored by using Whatman K6F silica gel 60 Å analytical TLC plates with UV detection ($\lambda = 254$ and 365 nm). Silica gel (60 Å, 32–63 μm) from EMD Science was used for column chromatography. Melting points (uncorrected) were measured by using Thomas Hoover capillary melting point apparatus. ^1H, ^{13}C ATP (APT = attached proton test), and ^{19}F NMR spectra were recorded by using a Varian Unity 400 spectrometer with a working frequency of 400.0 MHz. Chemical shifts were referenced to the residual resonance signal of the deuterated solvent. Low-resolution mass spectra were recorded on a Shimadzu GC–MS QP5050A instrument equipped with a direct probe (ionization 70 eV). High-resolution mass spectra (HRMS) were measured on a magnetic sector mass spectrometer using electron impact (EI) or electron spray ionization (ESI). Elemental analyses were measured by Atlantic Microlab, Inc. and ICT, Prague. Absorption spectra were recorded by using a Hitachi U-3010 double-beam spectrophotometer, accurate to ±0.3 nm. Steady-state and time-resolved fluorescence measurements were performed on a single-photon-counting spectrofluorimeter from Edinburgh Analytical Instruments. The solutions of the complexes were 30 μM in dichloromethane. Quantum yields were determined by using quinine sulfate (in 0.05 M H_2SO_4) as a standard. X-ray data were collected at room temperature on a Nonius Kappa CCD diffractometer using a graphite monochromator with $Mo_{K\alpha}$ radiation ($\lambda = 0.71073$ Å).

CCDC 287976–287979 contain the supplementary crystallographic data for this paper. These data can be obtained free of charge from The Cambridge Crystallographic Data Centre via www.ccdc.cam.ac.uk/data_request/cif.

Synthesis

*5-Bromo-8-*tert*-butoxycarbonyloxyquinoline (**3**)*: 4-Dimethylaminopyridine (DMAP; 136 mg, 1.12 mmol) was added at room temperature to a stirred suspension of 5-bromoquinolin-8-ol (5 g, 22.32 mmol) and di-*tert*-butyl dicarbonate (4.87 g, 22.32 mmol) in hexane (500 mL). The mixture was stirred for 5 h at room temperature, filtered by using a paper filter, and the filtrate was concentrated under vacuum to provide a crude product as a yellowish oil. The product was recrystallized from hexanes to yield white crystals (6.27 g, 87%). M.p. 86–88 °C; ^1H NMR ($CDCl_3$): $\delta =$ 1.60 (s, 9H), 7.42 (d, $J = 8.1$ Hz, 1H), 7.55 (dd, $J = 4.1$, 8.5 Hz, 1H), 7.81 (d, $J = 8.1$ Hz, 1H), 8.53 (dd, $J = 1.5$, 8.5 Hz, 1H), 8.96 ppm (dd, 1H, $J =$ 1.5, 4.1 Hz); ^{13}C APT NMR ($CDCl_3$): $\delta = 27.7$ (CH_3), 84.1 (C), 118.7 (C), 121.6 (CH), 122.8 (CH), 128.6 (C), 129.8 (CH), 135.9 (CH), 141.7 (C), 147.1 (C), 150.8 (CH), 151.6 ppm (C); EI-MS (direct insertion probe (DIP), 70 eV): *m*/*z* (%): 225 (100) [M^+−Boc]; elemental analysis calcd (%) for $C_{14}H_{14}BrNO_3$ (324.17): C 51.87, H 4.35, N 4.32, Br 24.65; found: C 51.62, H 4.57, N 4.15, Br 24.60.

*8-*tert*-Butoxycarbonyloxy-5-ethynylquinoline (**4**)*: A solution of **2** (3.0 g, 9.25 mmol) and diisopropylethylamine (DIPEA; 30 mL) in THF (300 mL) was purged with argon for 10 min at room temperature. Trimethylsilylacetylene (6.54 mL, 46.27 mmol) was added at room temperature under an argon atmosphere followed by addition of $[Pd(PPh_3)_4]$ (530 mg, 0.46 mmol) and CuI (88 mg, 0.46 mmol). The mixture was stirred for 24 h in a sealed tube under an argon atmosphere at 60 °C. The mixture was cooled to room temperature, poured into diethyl ether (300 mL), and filtered through a silica gel pad (10 g) by using diethyl ether (100 mL) as the eluent. The filtrate was concentrated under vacuum and the residue was redissolved in methanol (300 mL). KF (717 mg, 12.24 mmol) was added to the solution and the mixture was stirred for 3 h at room temperature. The reaction mixture was filtered using a paper filter, and water (300 mL) was added. Methanol was evaporated under vacuum at room temperature and the residue was extracted with dichloromethane (300 mL). The dichloromethane layer was separated, dried over anhydrous sodium sulfate, filtered, and concentrated under vacuum. The residue was purified by using column chromatography on silica gel (mobile

phase hexanes/acetone 9:1) to provide a white powder (1.72 g, 69%). The analytical sample was recrystallized from acetone/hexanes to provide white crystals. M.p. 116–118°C; ^{1}H NMR ($CDCl_3$): δ = 1.59 (s, 9H), 3.47 (s, 1H), 7.48 (d, J = 7.9 Hz, 1H), 7.52 (dd, J = 4.2, 8.5 Hz, 1H), 7.76 (d, J = 7.9 Hz, 1H), 8.63 (dd, J = 1.7, 8.5 Hz, 1H), 8.96 ppm (dd, J = 1.7, 4.2 Hz, 1H); ^{13}C APT NMR ($CDCl_3$): δ = 27.6 (CH_3), 80.0 (CH), 82.6 (C), 84.0 (C), 118.0 (C), 120.5 (CH), 122.5 (CH), 130.0 (C), 131.3 (CH), 134.5 (CH), 140.9 (C), 148.2 (C), 150.8 (CH), 151.6 ppm (C); EI-MS (DIP, 70 eV): m/z (%): 169 (100) [M^+−Boc]; elemental analysis calcd (%) for $C_{16}H_{15}NO_3$ (269.30): C 71.36, H 5.61, N 5.20; found: C 71.44, H 5.43, N 5.16.

General method A

Sonogashira–Hagihara coupling for preparation of ***5a,b,d–f***: A solution of **4** (400 mg, 1.49 mmol), haloarene (1.35 mmol), and DIEPA (4 mL) in THF (40 mL) was purged with argon for 10 min at room temperature. A mixture of solid [$Pd(PPh_3)_4$] (78 mg, 0.068 mmol) and CuI (13 mg, 0.068 mmol) was added into the solution under an argon atmosphere and the mixture was stirred at 60°C for 24 h. The reaction mixture was cooled to room temperature, diluted with diethyl ether (40 mL), and filtered through a silica gel pad (5 g) by using diethyl ether (40 mL) as the eluent. The filtrate was concentrated under vacuum and the residue was purified by using column chromatography on silica gel.

8-tert-*Butoxycarbonyloxy-5-[2-(4,6-dimethoxy-1,3,5-triazinyl) ethynyl]quinoline (**5a**)*: 2-Chloro-4,6-dimethoxy-1,3,5-triazine was used as the starting haloarene. Mobile phase for column chromatography: hexanes/acetone 4:1. Yield: 503 mg (83%). An analytical sample was recrystallized from acetone/hexanes to provide off-white crystals. M.p. 141–142°C; ^{1}H NMR ($CDCl_3$): δ = 1.60 (s, 9H), 4.12 (s, 6H), 7.55 (d, J = 7.9 Hz, 1H), 7.58 (dd, J = 4.3, 8.5 Hz, 1H), 7.97 (d, J = 7.9 Hz, 1H), 8.77 (dd, J = 1.7, 8.5 Hz, 1H), 8.99 ppm (dd, J = 1.7, 4.3 Hz, 1H); ^{13}C APT NMR ($CDCl_3$): δ = 27.7 (CH_3), 55.6 (CH_3), 84.2 (C), 87.0 (C), 91.8 (C), 116.3 (C), 120.6 (CH), 122.9 (CH), 130.4 (C), 133.0 (CH), 134.5 (CH), 141.0 (C), 149.7 (C), 151.1 (CH), 151.4 (C), 162.7 (C), 172.5 ppm (C); EI-MS (DIP, 70 eV): m/z (%): 308 (100) [M^+−Boc]; elemental analysis calcd (%) for $C_{21}H_{20}N_4O_5$ (408.41): C 61.76, H 4.94, N 13.72; found: C 61.80, H 5.08, N 13.67.

General method B

Sonogashira–Hagihara coupling for the preparation of ***5c,g–k***: A solution of **3** (1.0 g, 3.09 mmol), the acetylene derivative (3.09 mmol), and DIPEA (10 mL) in THF (100 mL) was purged with argon for 10 min at room temperature. A solid mixture of [$Pd(PPh_3)_4$] (180 mg, 0.155 mmol) and CuI (30 mg, 0.155 mmol) was added under an argon atmosphere and the mixture was stirred at 60°C for 24 h. The reaction mixture was cooled to room temperature, diluted with diethyl ether (100 mL), and filtered through a silica gel pad (10 g) by using diethyl ether (50 mL) as the eluent. The filtrate was concentrated under vacuum and the residue was purified by using column chromatography on silica gel (mobile phase: hexanes/acetone 9:1).

8-tert-*Butoxycarbonyloxy-5-(4-pyridylethynyl)quinoline (**5c**)*: 4-Ethynylpyridine hydrochloride was used as the starting acetylene derivative. Yield: 520 mg (49%) of a white crystalline compound. An analytical sample was recrystallized from dichloromethane/hexanes. M.p. 101–102°C; ^{1}H NMR ($CDCl_3$): δ = 7.47 (m, 2H), 7.54 (d, J = 7.8 Hz, 1H), 7.56 (dd, J = 4.1, 8.4 Hz, 1H), 7.82 (d, J = 7.8 Hz, 1H), 8.63–8.67 (m, 3H), 8.99 ppm (dd, J = 1.7, 4.1 Hz, 1H); ^{13}C APT NMR ($CDCl_3$): δ = 27.7 (CH_3), 84.1 (C), 90.1 (C), 91.8 (C), 117.9 (C), 120.6 (CH), 122.6 (CH), 125.5 (CH), 129.7 (C), 130.9 (C), 131.2 (CH), 134.2 (CH), 141.1 (C), 148.6 (C), 149.9 (CH), 150.9 (CH), 151.6 ppm (C); EI-MS (DIP, 70 eV): m/z (%): 246 (100) [M^+−Boc]; elemental analysis calcd (%) for $C_{21}H_{18}N_2O_3$ (346.38): C 72.82, H 5.24, N 8.09; found: C 72.40, H 5.24, N 8.01.

General method for the basic deprotection of a Boc derivative—preparation of 6a–c,e,f,h,k: Piperidine (0.1 mL, 1 mmol) was added to a stirred solution of Boc derivative (0.35 mmol) in dry CH_2Cl_2 (1 mL) at room temperature and the mixture was stirred for 5 min at the same temperature. The mixture was concentrated under vacuum and the residue was treated with acetone (5 mL). The resulting precipitate was isolated by using filtration and the filter cake was washed with acetone and dried to provide a product.

*8-Hydroxy-5-[2-(4,6-dimethoxy-1,3,5-triazinyl)ethynyl] quinoline (**6a**)*: Yellowish powder (79%); m.p. 228–230°C; ^{1}H NMR ($CDCl_3$): δ = 4.11 (s, 6H), 7.18 (d, J = 8.0 Hz, 1H), 7.60 (dd, J = 4.3, 8.5 Hz, 1H), 7.93 (d, J = 8.0 Hz, 1H), 8.75 (dd, J = 1.5, 8.5 Hz, 1H), 8.85 ppm (dd, J = 1.5, 4.3 Hz, 1H); ^{13}C APT NMR ($CDCl_3$): δ = 55.5 (CH_3), 88.9 (C), 90.8 (C), 108.4 (C), 110.1 (CH), 123.2 (CH), 129.7 (C), 134.9 (CH), 135.4 (CH), 137.8 (C), 148.7 (CH), 155.1 (C), 163.0 (C), 172.4 ppm (C); EI-MS (DIP, 70 eV): m/z (%): 308 (100) [M^+]; elemental analysis calcd (%) for $C_{16}H_{12}N_4O_3$ (308.29): C 62.33, H 3.92, N 18.17; found: C 62.61, H 3.96, N 18.16.

General method for the acidic deprotection of a Boc derivative—preparation of 7d,g,i–k: Trifluoroacetic acid (0.42 mL, 616 mg, 5.40 mmol) was added to a stirred solution of a Boc derivative (1.08 mmol) in dry CH_2Cl_2 (40 mL) under an argon atmosphere at room temperature. The mixture was stirred for 24 h at room temperature under an argon atmosphere. The solvent was evaporated under vacuum and the residue was recrystallized from acetone.

*5-(4-Cyanophenylethynyl)-8-hydroxyquinolinium trifluoroacetate (**7d**)*: Yellow powder (99%); m.p. 181–182°C; ^{1}H NMR ([D_6]DMSO): δ = 7.21 (d, J = 8.1 Hz, 1H), 7.82 (dd, J = 4.3, 8.4 Hz, 1H), 7.85–7.96 (m, 5H), 8.86 (dd, J = 1.5, 8.4 Hz, 1H), 9.00 ppm (dd, J = 1.5, 4.3 Hz, 1H); ^{13}C APT NMR ([D_6]DMSO): δ = 90.7 (C), 91.7 (C), 108.9 (C), 110.7 (C), 112.4 (CH), 118.5 (C), 123.3 (CH), 127.4 (C), 129.1 (C), 132.0 (CH), 132.6 (CH), 133.5 (CH), 136.1 (CH), 136.6 (C), 148.3 (CH), 154.5 (C), 158.2 ppm (C; CF_3COO^-, J_{CF} = 36.6 Hz); EI-MS (DIP, 70 eV): m/z (%): 270 (100) [M^+−CF_3COOH]; elemental analysis calcd (%) for $C_{20}H_{11}F_3N_2O_3 \cdot {}^3/_4CH_2Cl_2$ (448.01): C 55.64, H 2.79, N 6.25; found: C 55.82, H 2.53, N 5.94.

8-(Benzyloxy)-5-(4,4,5,5-tetramethyl[1,3,2]dioxaborolan-2-yl)quinoline (9): A flame-dried screw-cap flask was loaded with 8-(benzyloxy)-5-bromoquinoline (4.713 g, 15.00 mmol), dry Et_3N (15.00 mL), and dry THF (75.00 mL). The solution was purged with argon for 10 min, then 4,4,5,5-tetramethyl-1,3,2-dioxaborolane (2.400 mL, 2.112 g, 16.50 mmol) and [$Pd(PPh_3)_4$] (0.520 g, 0.45 mmol) were added. The mixture was stirred for 24 h at 100°C under an argon atmosphere, cooled to room temperature, diluted with diethyl ether (100 mL), and filtered through a silica gel pad by using diethyl ether as the eluent. The filtrate was concentrated under vacuum, and the residue was purified by using column chromatography on silica gel (mobile phase: hexanes/acetone 4:1) to provide the product as a yellowish oil (5.17 g, 95%), which was recrystallized from acetone/hexanes to provide white crystals. M.p. 123–124°C; ^{1}H NMR ($CDCl_3$): δ = 1.38 (s, 12H), 5.47 (s, 2H), 7.01 (d, J = 7.9 Hz, 1H), 7.27 (m, 1H), 7.34 (m, 2H), 7.47 (dd, J = 4.1, 8.6 Hz, 1H), 7.50 (m, 2H), 7.99 (d, J = 7.9 Hz, 1H), 8.96 (dd, J = 1.8, 4.1 Hz, 1H), 9.1 ppm (dd, J = 1.7, 8.6 Hz, 1H); ^{13}C APT NMR ($CDCl_3$): δ = 24.9 (CH_3), 70.5 (CH_2), 83.6 (C), 109.1 (CH), 121.8 (CH), 127.0 (CH), 127.8 (CH), 128.6 (CH), 133.4 (C), 136.7 (CH), 137.0 (CH), 140.4 (C), 148.9 (CH), 156.9 ppm (C); EI-MS (DIP, 70 eV): m/z (%): 361 (22) [M^+], 284 (17) [M^+−Ph], 255 (25) [M^+−BnO], 91 (100) [tropylium$^+$].

General method C

Suzuki–Miyaura coupling for the preparation of ***10a–e,j,k***: Compound **4** (1.242 g, 3.44 mmol), haloarene (3.44 mmol), tetrabutylammonium chloride (0.110 g, 0.37 mmol), and tetrakis(triphenylphosphine) palladium (0.180 g, 0.16 mmol) were added to an air-free two-phase mixture of toluene (25 mL) and an aqueous 1 M K_2CO_3 solution (25 mL). The reaction mixture was intensively stirred under an argon atmosphere at 90°C for 24 h. The organic layer was separated and the aqueous phase was extracted with toluene (3×30 mL). The organic layers were combined, washed with water (2×50 mL), and dried with anhydrous Na_2SO_4. The solvent was evaporated and the residue was dissolved in dichloromethane and filtered over silica gel by using 25% methanol/dichloromethane as the mobile phase.

*8-(Benzyloxy)-5-[2-(4,6-dimethoxy-1,3,5-triazinyl)] quinoline (**10a**)*: 2-Chloro-4,6-dimethoxy-1,3,5-triazine was used as the starting aryl halide. Mobile phase for chromatography: hexanes/acetone 7:3. Yield: 0.190 g (51%) of white solid. The analytical sample was obtained by crystalliza-

tion from an acetone/hexanes mixture to provide white crystals. M.p. 122–123 °C; ^{1}H NMR ($CDCl_3$): δ = 4.13 (s, 6H), 5.53 (s, 2H), 7.11 (d, J = 8.4 Hz, 1H), 7.30 (m, 1H), 7.37 (m, 2H), 7.53 (m, 2H), 7.55 (dd, J = 4.0, 8.9 Hz, 1H), 8.53 (d, J = 8.4 Hz, 1H), 9.01 (dd, J = 1.7, 4.0 Hz, 1H), 9.72 ppm (dd, J = 1.7, 8.9 Hz, 1H); ^{13}C APT NMR ($CDCl_3$): δ = 55.2 (CH_3), 70.8 (CH_2), 108.6 (CH), 122.4 (CH), 123.9 (C), 127.0 (CH), 127.9 (CH), 128.2 (C), 128.6 (CH), 132.5 (CH), 134.8 (CH), 136.1 (C), 140.3 (C), 149.1 (CH), 157.7 (C), 172.3 (C), 175.5 ppm (C); EI-MS (DIP, 70 eV): m/z (%): 374 (21) [M^+], 297 (14), 268 (17) [M^+−BnO], 91 (100) [tropylium$^+$].

General method D

Suzuki–Miyaura coupling for the preparation of ***10f–h,l–n***: 8-(Benzyloxy)-5-bromoquinoline (1.057 g, 3.37 mmol), a phenylboronic acid derivative (3.40 mmol), tetrabutylammonium chloride (TBACl; 0.110 g, 0.37 mmol), and tetrakis(triphenylphosphine) palladium (0.180 g, 0.16 mmol) were added to an air-free two-phase mixture of toluene (30 mL) and an aqueous 1 M K_2CO_3 solution (30 mL). The resulting mixture was intensively stirred under an argon atmosphere at 90 °C for 24 h. The organic layer was separated and the aqueous phase was extracted with toluene (3 × 30 mL). The organic layers were combined, washed with water (2 × 50 mL), and dried with anhydrous Na_2SO_4. The solvent was evaporated and the residue was dissolved in dichloromethane and filtered over silica gel by using 25% methanol/dichloromethane as the mobile phase. The crude product was purified by recrystallization or column chromatography.

*8-(Benzyloxy)-5-(4-cyanophenyl)quinoline (**10f**)*: 4-Cyanophenylboronic acid was used as the starting material for the cross-coupling. The resulting compound was recrystallized from ethanol to provide white crystals (0.536 g, 46%). M.p. 180–181 °C; ^{1}H NMR ($CDCl_3$): δ = 5.51 (s, 2H), 7.09 (d, J = 7.9 Hz, 1H), 7.32 (m, 2H), 7.38 (m, 2H), 7.43 (dd, J = 4.3, 8.5 Hz, 1H), 7.51–7.56 (m, 4H), 7.76 (m, 2H), 8.11 (dd, J = 1.8, 8.5 Hz, 1H), 9.03 ppm (dd, J = 1.8, 4.3 Hz, 1H); ^{13}C APT NMR ($CDCl_3$): δ = 70.9 (CH_2), 109.4 (CH), 111.2 (C), 118.8 (C), 122.0 (CH), 127.1 (CH), 127.2 (C), 127.6 (CH), 128.0 (CH), 128.3 (C), 128.7 (CH), 130.3 (C), 130.8 (CH), 132.3 (CH), 133.4 (CH), 136.7 (CH), 140.6 (C), 144.3 (C), 149.5 (CH), 149.7 (C), 153.1 (C); EI-MS (DIP, 70 eV): m/z (%): 336 (20) [M^+], 259 (7) [M−$C_6H_6^+$], 230 (11) [M−benzaldehyde$^+$], 91 (100) [tropylium$^+$].

General method for the deprotection of the benzyl derivative by catalytic transfer hydrogenation—preparation of the ligands 11a–n: 1,4-Cyclohexadiene (0.500 mL, 5.4 mmol) was added in one portion to a mixture of the benzyl derivatives **10** (1.80 mmol) and 10% Pd/C catalyst (300 mg) in degassed isopropanol (30 mL). The mixture was heated at 110 °C for 3 h in a screw-cap flask. The solution was cooled to room temperature and filtered over filter paper to remove the catalyst. The solvent was evaporated and the crude product was purified by means of recrystallization or column chromatography.

*8-Hydroxy-5-[2-(4,6-dimethoxy-1,3,5-triazinyl)]quinoline (**11a**)*: 8-(Benzyloxy)-5-[2-(4,6-dimethoxy-1,3,5-triazinyl)]quinoline (**10a**) was used as the starting material. The resulting product was recrystallized from ethanol to give white crystals (0.84 g, 59%). M.p. 227–229 °C; ^{1}H NMR ($CDCl_3$): δ = 4.15 (s, 6H), 7.25 (d, J = 8.3 Hz, 1H), 7.56 (dd, J = 4.1, 8.9 Hz, 1H), 8.76 (d, J = 8.3 Hz, 1H), 8.81 (dd, J = 1.6, 4.1 Hz, 1H), 9.89 ppm (dd, J = 1.6, 8.9 Hz, 1H); ^{13}C APT NMR ($CDCl_3$): δ = 55.1 (CH_3), 109.2 (CH), 122.3 (C), 122.9 (CH), 127.8 (C), 134.0 (CH), 136.0 (CH), 138.4 (C), 147.6 (CH), 156.5 (C), 172.6 (C), 175.7 ppm (C); EI-MS (DIP, 70 eV): m/z (%): 284 (100) [M^+], 269 (50), 212 (33).

General method for the preparation of complexes 1a–k: A 0.05 M aqueous solution of $AlCl_3$·6H_2O (0.07 mol) was added to a boiling solution of the ligand (free base or TFA) (0.210 mmol) in ethanol (15 mL). The mixture was left at reflux for 1 h, neutralized with Et_3N and cooled to room temperature. The precipitated aluminum complex was collected by using filtration and the filter cake was washed with water, ethanol, and diethyl ether to provide the desired product. Complexes **1a–k** can be recrystallized from ethanol or dichloromethane/hexanes.

*Aluminum(III) tris[5-(4-dimethylaminophenylethynyl)]-8-quinolinolate (**1k**)*: Orange solid (84%); m.p. 245–247 °C (decomp); ^{1}H NMR ($CDCl_3$): δ = 2.98 (s, 12H; CH_3), 2.99 (s, 6H; CH_3), 6.67 (m, 6H), 7.07 (m, 3H), 7.24 (dd, J = 1.5, 4.9 Hz, 1H), 7.30 (dd, J = 4.9, 8.3 Hz, 1H), 7.40–7.50 (m, 7H), 7.54 (dd, J = 4.9, 8.3 Hz, 1H), 7.75 (m, 3H), 8.73 (dd, J = 1.5, 8.3 Hz, 1H), 8.77 (dd, J = 1.5, 8.3 Hz, 1H), 8.81 (m, 2H), 8.85 ppm (dd, J = 1.5, 4.9 Hz, 1H); ^{13}C APT NMR ($CDCl_3$): δ = 40.4 (CH_3), 84.0 (C), 84.3 (C), 84.7 (C), 92.8 (C), 93.1 (C), 93.4 (C), 106.3 (C), 106.4 (C), 106.7 (C), 110.3 (C), 110.5 (C), 110.7 (C), 111.9 (CH), 112.7 (CH), 113.2 (CH), 113.8 (CH), 121.5 (CH), 122.0 (CH), 122.2 (CH), 129.7 (C), 129.9 (C), 130.0 (C), 132.5 (CH), 134.7 (CH), 134.9 (CH), 135.2 (CH), 138.8 (CH), 138.9 (CH), 139.15 (C), 139.24 (CH), 139.8 (C), 142.7 (CH), 144.9 (CH), 145.2 (CH), 149.9 (C), 149.98 (C), 150.04 (C), 158.7 (C), 159.0 (C), 159.2 ppm (C); HRMS (ESI): m/z calcd for $C_{57}H_{46}AlN_6O_3$ [M+H$^+$]: 889.3447; found: 889.3487; elemental analysis calcd (%) for $C_{57}H_{45}AlN_6O_3$·5H_2O (979.08): C 69.93, H 5.66, N 8.58; found: C 70.17, H 5.02, N 8.38.

General method for the preparation of the aluminum complexes 2a–n: A mixture of the ligand (0.15 mmol) and $AlCl_3$·6H_2O (12 mg, 0.05 mmol) in degassed ethanol (5 mL) was left at reflux for 3 h. The mixture was cooled to room temperature and neutralized by using triethylamine. Water (10 mL) was added and the precipitated complex was filtered off. The filter cake was washed thoroughly with water, ethanol, and diethyl ether, and dried under vacuum to provide the desired product.

*Aluminum(III) tris[5-[2-(4,6-dimethoxy-1,3,5-triazinyl)]-8-quinolinolate} (**2a**)*: Yellow solid (28 mg, 95%); m.p. >260 °C; ^{1}H NMR ($CDCl_3$): δ = 4.11 (s, 6H), 4.12 (s, 6H), 4.13 (s, 6H), 7.15 (m, 2H), 7.19 (d, J = 8.5 Hz, 1H), 7.29 (dd, J = 1.5, 4.7 Hz, 1H), 7.38 (dd, J = 4.7, 8.7 Hz, 1H), 7.55 (dd, J = 4.7, 8.7 Hz, 1H), 7.63 (dd, J = 4.7, 8.7 Hz, 1H), 8.83 (dd, J = 1.5, 4.7 Hz, 1H), 8.86–8.94 (m, 3H), 8.96 (d, J = 8.5 Hz, 1H), 10.17 (dd, J = 1.5, 8.7 Hz, 1H), 10.21 (dd, J = 1.5, 8.7 Hz, 1H), 10.26 ppm (dd, J = 1.5, 8.7 Hz, 1H); HRMS (ESI): m/z calcd for $C_{42}H_{33}AlN_{12}O_9$ [M+H$^+$]: 877.2387; found: 877.2409.

Calculation of the energy-gap law correlation data: Values for the emission energy (E_{em}) and the radiative (k_r) and nonradiative (k_{nr}) rate decay rate constants were calculated by using the Equations (1)–(3):

$$E_{em} = h\nu_{max} = \frac{hc}{\lambda_{max}} \quad (1)$$

$$k_r = \frac{\phi}{\tau_F} \quad (2)$$

$$k_{nr} = \frac{1}{\tau_F} - k_r \quad (3)$$

Estimation of the HOMO/LUMO energy levels for the complexes: The HOMO and LUMO energies were calculated by using a commonly accepted procedure.[34] According to this, the value for ferrocene (Fc) with respect to the zero vacuum level is estimated as −4.8 eV, determined from −4.6 eV for the standard electrode potential E° of a normal hydrogen electrode (NHE) on the zero vacuum level, and 0.2 V for Fc versus NHE. Thus, the values for the HOMO and LUMO levels were obtained through Equations (4) and (5) as follows:

$$\text{HOMO} = -(E^{ox} + 4.8)\ \text{eV} \quad (4)$$

$$\text{LUMO} = -(E^{red} + 4.8)\ \text{eV} \quad (5)$$

in which E^{ox} and E^{red} are the redox potentials referenced against ferrocene.

Construction of the devices: The OLEDs were fabricated on Applied Films Corp ITO-coated glass substrates (150–200 nm thick; resistance, $R \approx 20\ \Omega$/square). The ITO-coated substrates, which served as the anode, were degreased by a detergent and organic solvents and then UV-ozone cleaned to increase the ITO work function. The organic layers, CsF electron injection buffer layer, and Al cathode were deposited by thermal evaporation in a high-vacuum ($\approx 10^6$ torr) chamber installed in an Ar-filled glove-box (<1 ppm O_2, H_2O). The organic layers consisted of a 5 nm-thick copper phthalocyanine (CuPc) layer, a 60 nm-thick *N,N′*-diphenyl-*N,N′*-bis(1-naphthylphenyl)-1,1′-biphenyl-4,4′-diamine (α-NPD) layer, and a 50 nm-thick layer of the Alq_3 derivative. The cathode consist-

ed of a ≈1 nm-thick CsF layer and a ≈150 nm-thick Al layer. The deposition rate of the organic layers was 0.05–0.1 nm s^{-1}, controlled by a calibrated quartz-crystal thickness monitor. The CsF layer was deposited at ≈0.01 nm sec^{-1}. The Al was deposited at 0.5–0.7 nm sec^{-1} through a mask of 3.0 mm diameter holes. The Alq_3 derivatives that could not be thermally evaporated were dissolved in toluene and embedded in a poly(9-vinylcarbazole) (PVK) (10 mg mL^{-1} in toluene) matrix. The "1×1" ITO substrates were then spin coated at 4000 rpm with poly(3,4-ethylenedioxythiophene) (PEDOT)/poly(styrene sulfonate) (PSS) and baked at 150°C for 60 min. The Alq_3 derivative/PVK blend was then spin coated at 2000 rpm onto the PEDOT/PSS. A 30 nm-thick layer of 2,9-dimethyl-4,7-diphenyl-1,10-phenanthroline (BCP), a hole-blocking electron-transporting layer, was then thermally evaporated onto the spin-coated Alq_3 derivative-doped PVK. CsF and Al films were deposited as described above.

Characterization of the OLEDs: The current–voltage and electroluminescence intensity–voltage curves were measured by using a Keithley 2000 digital multimeter (DMM) and Minolta L100 luminance meter. The EL spectra were measured by using an OceanOptics Chem-2000 spectrometer. The external maximum efficiency of the diodes was determined by using Equation (6):

$$\eta = \frac{\pi e}{K_m hc}\frac{L}{J}\frac{\int F(\lambda)d\lambda}{\int \frac{F(\lambda)y(\lambda)d\lambda}{\lambda}} \quad (6)$$

in which L is the measured forward-directed luminance [cd m^{-2}], J is the current density [A m^{-2}], K_m is the maximum luminous efficacy (namely, 680 Lm W^{-1}), $y(\lambda)$ is the normalized photopic spectral response function, $F(\lambda)$ is the electroluminescence emission spectrum for the device, and λ is the wavelength.

Acknowledgements

Financial support from the NSF (NER Grant 0304320, DMR Grant 0306117 to P.A.), the Alfred P. Sloan Research Foundation to P.A., the BGSU (Technology Innovations Enhancement grant to P.A.), and the M^c Master Endowment for a M^e Master fellowship to V.M. is gratefully acknowledged. Ames Laboratory is operated by Iowa State University for the US Department of Energy under contract W-7405-Eng-82. The work in Ames was supported by the Director for Energy Research, Office of Basic Energy Sciences. We thank Manuel Palacios for his help with the cover graphic.

[1] S. M. Kelly in *Flat Panel Displays: Advanced Organic Materials* (series Ed.: J. A. Connor), The Royal Society of Chemistry, Cambridge, **2000**.
[2] J. Shinar, *Organic Light-Emitting Devices—A Survey*, Springer, Berlin, **2003**.
[3] A. B. Holmes, *Nature* **2003**, *421*, 800–801.
[4] L. S. Hung, C. H. Chen, *Mater. Sci. Eng. R* **2002**, *39*, 143–222.
[5] E. Holder, B. M. W. Langeveld, U. S. Schubert, *Adv. Mater.* **2005**, *17*, 1109–1121.
[6] S. Naka, H. Okada, H. Onagawa, *Mol. Electron. Bioelectron.* **2000**, *11*, 70–77.
[7] C. W. Tang, S. A. VanSlyke, *Appl. Phys. Lett.* **1987**, *51*, 913–915.
[8] V. Bulovic, M. A. Baldo, S. R. Forrest in *Organic Electronic Materials* (Eds.: R. Farchioni, G. Grosso), Springer, Berlin, **2001**, pp. 391–439, and references therein.
[9] C. H. Chen, J. Shi, *Coord. Chem. Rev.* **1998**, *171*, 161–174.
[10] a) A. Curioni, M. Boero, W. Andreoni, *Chem. Phys. Lett.* **1998**, *294*, 263–271; b) M. Sugimoto, S. Sakaki, K. Sakanoue, M. D. Newton, *J. Appl. Phys.* **2001**, *90*, 6092–6097; c) M. D. Halls, H. B. Schlegel, *Chem. Mater.* **2001**, *13*, 2632–2640; d) B. C. Lin, C. P. Cheng, Z.-Q. You, C.-P. Hsu, *J. Am. Chem. Soc.* **2005**, *127*, 66–67.
[11] "Luminescent Metal Complexes: Diversity of Excited States": A. K. H. Vogler in *Topics in Current Chemistry, Vol. 241, Transition Metal and Rare Earth Compounds: Excited States, Transitions, Interactions I* (Ed.: H. Yersin), Springer, Berlin, **2001**.
[12] L. S. Sapochak, A. Padmaperuma, N. Washton, F. Endrino, G. T. Schmett, J. Marshall, D. Fogarty, P. E. Burrows, S. R. Forrest, *J. Am. Chem. Soc.* **2001**, *123*, 6300–6307.
[13] M. Sugimoto, M. Anzai, K. Sakanoue, S. Sakaki, *Appl. Phys. Lett.* **2001**, *79*, 2348–2350.
[14] a) T. A. Hopkins, K. Meerholz, S. Shaheen, M. L. Anderson, A. Schmidt, B. Kippelen, A. B. Padias, J. H. K. Hall, N. Peyghambarian, N. R. Armstrong, *Chem. Mater.* **1996**, *8*, 344–351; b) J.-A. Cheng, C. H. Chen, C. H. Liao, *Chem. Mater.* **2004**, *16*, 2862–2868.
[15] P. E. Burrows, Z. Shen, V. Bulovic, D. M. McCarty, S. R. Forrest, J. A. Cronin, M. E. Thompson, *J. Appl. Phys.* **1996**, *79*, 7991–8006.
[16] M. Matsumura, T. Akai, *Jpn. J. Appl. Phys. Part 1* **1996**, *35*, 5357–5360.
[17] S. Anderson, M. S. Weaver, A. J. Hudson, *Synth. Met.* **2000**, *111–112*, 459–463.
[18] a) P. S. Bryan, F. V. Lovecchio, S. A. VanSlyke (assignee: Eastman Kodak Company), United States Patent and Trademark Office (USPTO), US 5,141,671, **1992**; b) S. A. VanSlyke (assignee: Eastman Kodak Company), USPTO, US patent, US 5,151,629, **1992**; c) L. S. Sapochak, P. E. Burrows, D. Garbuzov, D. M. Ho, S. R. Forrest, M. E. Thompson, *J. Phys. Chem.* **1996**, *100*, 17766–17771.
[19] R. Pohl, P. Anzenbacher, Jr., *Org. Lett.* **2003**, *5*, 2769–2772.
[20] R. Pohl, V. A. Montes, J. Shinar, P. Anzenbacher, Jr., *J. Org. Chem.* **2004**, *69*, 1723–1725.
[21] R. Prasad, H. L. D. Coffer, Q. Fernando, H. Freiser, *J. Org. Chem.* **1965**, *30*, 1251–1251.
[22] Y. Nakano, D. Imai, *Synthesis* **1997**, 1425–1428.
[23] a) M. Coelle, R. E. Dinnebier, W. Bruetting, *Chem. Commun.* **2002**, *23*, 2908–2909; b) M. Coelle, S. Forero-Lenger, J. Gmeiner, W. Bruetting, *Phys. Chem. Chem. Phys.* **2003**, *5*, 2958; c) M. Coelle, W. Bruetting, *Phys. Status Solidi A* **2004**, *201*, 1095–1115; d) M. Utz, M. Nandagopal, M. Mathai, F. Papadimitrakopoulos, *Appl. Phys. Lett.* **2003**, *83*, 4023–4025.
[24] A. Curioni, W. Andreoni, *J. Am. Chem. Soc.* **1999**, *121*, 8216–8220.
[25] M. Utz, C. Chen, M. Morton, F. Papadimitrakopoulos, *J. Am. Chem. Soc.* **2003**, *125*, 1371–1375.
[26] B. C. Baker, D. T. Sawyer, *Anal. Chem.* **1968**, *40*, 1945–1951.
[27] N. J. Turro, *Modern Molecular Photochemistry*, Benjamin–Cummings Publishing, Menlo Park, **1978**.
[28] B. R. Henry, W. Siebrand in *Organic Molecular Photophysics, Vol. 1* (Ed.: J. B. Birks), Wiley, London, **1973**.
[29] C. Hansch, A. Leo, R. W. Taft, *Chem. Rev.* **1991**, *91*, 165–195.
[30] M. B. Smith, J. March, *March's Advanced Organic Chemistry: Reactions, Mechanisms, and Structure*, 5th ed., Wiley-Interscience, New York, **2001**.
[31] a) A. Bard, R. Faulkner, *Electrochemical Methods—Fundamentals and Applications*, 2nd ed., Wiley, New York, **2001**; b) A. Benniston, A. Harriman, D. Lawrie, A. Mayeux, K. Rafferty, O. Russell, *Dalton Trans.* **2003**, 4762–4769; c) M. Hissler, A. Harriman, A. Khatyr, R. Ziessel, *Chem. Eur. J.* **1999**, *5*, 3366–3381; d) P. Roy, M. Saha, T. Okajima, T. Ohsaka, *Electroanalysis* **2004**, *16*, 289–297; e) T. Mizoguchi, R. N. Adams, *J. Am. Chem. Soc.* **1962**, *84*, 2058–2061; f) E. Bosch, J. Kochi, *J. Org. Chem.* **1994**, *59*, 5573–5586.
[32] J. D. Anderson, E. M. Mc Donald, P. A. Lee, M. L. Anderson, E. L. Ritchie, H. K. Hall, T. Hopkins, E. A. Mash, J. Wang, A. Padias, S. Thayumavan, S. Barlow, S. R. Marder, G. E. Jabbour, S. Shaheen, B. Kippelen, N. Peyghambarian, R. M. Wightman, N. R. Armstrong, *J. Am. Chem. Soc.* **1998**, *120*, 9646–9655.
[33] I. G. Hill, A. Kahn, Z. G. Soos, R. A. Pascal, *Chem. Phys. Lett.* **2000**, *327*, 181–188.
[34] J. Pommerehne, H. Vestweber, W. Guss, R. Mahrt, H. Bässler, M. Porsch, J. Daub, *Adv. Mater.* **1995**, *7*, 551–554.
[35] H. Mu, H. Shen, D. Klotzkin, *Solid-State Electron.* **2004**, *48*, 2085–2088.
[36] S. A. Odom, S. R. Parkin, J. E. Anthony, *Org. Lett.* **2003**, *5*, 4245–4248.

[37] A. Van Dijken, J. J. A. M. Bastiaansen, N. M. M. Kiggen, B. M. W. Langeveld, C. Rothe, A. Monkman, I. Bach, P. Stössel, K. Brunner, *J. Am. Chem. Soc.* **2004**, *126*, 7718–7727.

[38] a) L. Zou, V. Savvate'ev, J. Booher, C.-H. Kim, J. Shinar, *Appl. Phys. Lett.* **2001**, *79*, 2282–2284; b) K. O. Cheon, J. Shinar, *Appl. Phys. Lett.* **2003**, *83*, 2073–2075.

Received: November 11, 2005
Published online: April 18, 2006

